Cell-Specific Regulation of Intestinal Immunity.

Minjeong Shin, Reegan J. Willms, Lena Ocampo Jones, Kristina Petkau, Andrew Panteluk, Edan Foley[1].

Department of Medical Microbiology and Immunology, Faculty of Medicine and Dentistry, University of Alberta, Edmonton, AB T6G 2S2, Canada.

1: Corresponding author.

Edan Foley: efoley@ualberta.ca

ABSTRACT

The intestinal epithelium contains secretory and absorptive cell lineages that develop from undifferentiated progenitor cells. Despite the collective importance of these cells to host responses against microbial invaders, little is known about the contributions of immune responses in individual cell types to the maintenance of intestinal homeostasis. In this study, we asked how inhibition of immune pathway activity exclusively in progenitor cells, or in differentiated enterocytes, affects midgut homeostasis in adult *Drosophila*. We found that blocking immune activity in enterocytes rendered flies more tolerant of *Vibrio cholerae* infection, had negligible effects on the gut bacterial microbiome, and significantly affected metabolism. In contrast, inhibition of immune activity in progenitors rendered flies less tolerant of *Vibrio* infections, modified host association with *Lactobacillus* symbionts, and blocked growth and renewal in the midgut epithelium. Together, these data uncover substantial cell type-specific contributions of epithelial immunity to adult intestinal homeostasis.

INTRODUCTION

Intestinal defenses are critical for the neutralization of threats posed by resident, or transient microbes (1). Antimicrobial protections include physical barriers, constructed from dense polymeric materials, such as mucins or the chitinous peritrophic matrix, as well as tight cell-cell contacts that prevent paracellular leakage of potentially harmful molecules. In addition to barrier defenses, host-derived reactive oxygen species eliminate invasive microbes in a rather indiscriminate manner that can lead to collateral damage of host tissue. Finally, immune systems rely on intra- and extracellular receptors that survey the intestinal environment for molecular patterns of the gut microbial content (2). Detection of microbial signatures activates evolutionarily conserved host defenses that prevent microbial invasion of interstitial tissue.

Drosophila melanogaster is a valuable system to characterize molecular regulation of intestinal immune responses. The fly posterior midgut shares numerous similarities with the vertebrate small intestine, and is highly amenable to the modification of gene expression in defined intestinal cells (3). Similar to vertebrates, the fly midgut is maintained by a basal population of progenitor cells composed of intestinal stem cells that mainly divide asymmetrically to generate a new stem cell and a transient cell type – the enteroblast (4, 5). Enteroblasts frequently respond to signals from the Notch pathway to generate absorptive enterocytes (6, 7), a large, differentiated cell that undergoes several rounds of endoreplication, and occupies the bulk of the epithelial volume. Less frequently, stem cells generate secretory enteroendocrine cells, either indirectly via enteroblasts that do not receive Notch signals, or more directly via an enteroendocrine intermediary (8–10). As with vertebrates, stem cell division is regulated by mitogenic cues from pathways that include EGF, Wnt, and JAK-STAT, and the rate of ISC division is tuned to the rate of epithelial damage (11, 12). In the absence of an extrinsic stressor, stem cells divide approximately once every two weeks in adult females (4, 13). However, damage to the midgut activates repair pathways that shift ISC proliferation rates. In this case, molecular cues from damaged cells accelerate ISC division to generate a pool of cells that replenishes damaged structures and maintains the epithelial barrier.

In the fly intestine, bacterial DAP-type peptidoglycan (PGN) activates the Immune Deficiency (IMD) pathway, a germline-encoded antibacterial defense with similarities to the mammalian TNF pathway (14–16). IMD regulates approximately 50% of the intestinal transcriptional response to the microbiota (17), and alterations in immune activity are associated with effects on the composition and load of the gut microbiota (15, 17–20). Similar to digestive processes, the IMD pathway displays hallmarks of cellular, and regional specialization (21–23). In the anterior of the intestine, IMD activation requires the extracellular receptor, PGRP-LC, that detects polymeric PGN, and activates antibacterial defenses in large, differentiated cells (24). In the posterior midgut, IMD activation requires PGRP-LE (24, 25), an intracellular sensor that detects monomeric PGN (26), and induces the expression of immune regulatory gene products.

Though advances have been made in understanding molecular and spatial regulation of intestinal IMD activity, few studies have asked if IMD executes distinct roles in undifferentiated progenitors compared to their differentiated progeny. We considered this an important question to address, as IMD pathway components are expressed and active in midgut progenitors (27–29), and germline-encoded immune pathways have critical homeostatic roles in the intestinal progenitor cells of other organisms. For example, mouse stem cells express the NOD2 and TLR4 bacterial sensors, and both receptors contribute to the regulation of stem cell viability (30–33). Likewise, microbiota-dependent cues act through the TLR pathway component, MyD88, to regulate growth and differentiation in the zebrafish larval epithelium (34, 35). Given the evolutionary conservation of intestinal homeostatic pathways, and the genetic accessibility of *Drosophila*, we believe the adult fly is an excellent system to characterize links between immune activity and epithelial homeostasis.

To identify cell-specific functions for IMD in the adult midgut, we generated a transgenic *Drosophila* line that allows inducible inhibition of IMD in defined cell types. With this line, we determined the physiological consequences of IMD inactivation exclusively in progenitors or in enterocytes. Our results revealed significant differences between the contributions of enterocyte IMD and progenitor cell IMD to intestinal homeostasis. Inhibition of IMD in enterocytes extended the lifespan of adults challenged with *Vibrio cholerae*, did not affect composition of the intestinal microbiome, but had significant effects on triglyceride metabolism. In contrast,

inhibition of IMD in progenitors shortened the lifespan of flies challenged with *Vibrio cholerae*, impacted the representation of *Lactobacillus* symbionts within the microbiota, and significantly impaired the growth and differentiation of intestinal stem cells. Combined, these data uncover fundamental differences between immune activity in progenitor cells, and their differentiated progeny, and provide an accessible model to dissect cell-specific contributions of epithelial immunity to health and viability.

RESULTS

Cell-specific effects of IMD on host responses to bacterial infection.

IMD activation requires proteolytic removal of the N-terminal thirty amino acids from the Imd protein by the caspase Dredd, and expression of a non-cleavable Imd (ImdD30A) prevents signal transduction through the IMD pathway (36). Thus, expression of ImdD30A in the adult fat body blocks infection-dependent expression of the IMD-responsive antimicrobial peptide, *diptericin* (Fig. S1A). To determine how cell-specific inactivation of IMD impacts survival after oral infection with *V.cholerae*, we used the TARGET gene expression system (37) to express ImdD30A exclusively in intestinal progenitors (*esg^{ts}/D30A*), or in differentiated enterocytes (*Myo1A^{ts}/D30A*). We chose *V. cholerae* for these studies, as previous work showed that IMD activity contributes to *V. cholerae*-dependent mortality (38). When we blocked IMD in progenitors, we found that flies infected with *V. cholerae* died significantly faster than control *esg^{ts}/+* flies (Fig. S1B). Conversely, enterocyte-specific suppression of IMD extended the survival of infected flies relative to *Myo1A^{ts}/+* controls (Fig. S1C). Notably, we detected equal loads of *V. cholerae* in *esg^{ts}/D30A* flies and *Myo1A^{ts}/D30A* flies relative to their respective controls (Fig. S1D and E). We also looked at the impacts of *esg^{ts}/D30A* and *Myo1A^{ts}/D30A* on feeding rates, a possible modifier of host colonization by *V. cholerae*. In these experiments, we found that *esg^{ts}/D30A* flies and *Myo1A^{ts}/D30A* flies consumed equal amounts of liquid (Fig. S1F and G), or solid (Fig. S1H and I) food as their respective controls, suggesting that IMD has cell-specific impacts on host tolerance of an enteric pathogen.

Effects of cell-specific IMD inactivation on the intestinal microbiome.

Given the differential impacts of enterocyte and progenitor IMD activity on host survival of a pathogenic bacteria, we asked if IMD also modifies interactions with symbiotic bacteria in a cell-specific fashion. To answer this question, we generated axenic populations of *esg^{ts}/+*, *esg^{ts}/D30A*, *Myo1A^{ts}/+* and *Myo1A^{ts}/D30A* embryos (Fig. 1A). We raised the embryos at 21°C in a sterile environment until adulthood to prevent unwanted expression of *imdD30A* during development. We simultaneously fed all axenic adults a homogenate prepared from our lab wild-type flies to ensure that all genotypes had identical starting microbiomes. We then transferred the flies to

29°C to induce ImdD30A expression in progenitors (*esg^{ts}/D30A*) or enterocytes (*Myo1A^{ts}/D30A*), and performed triplicate 16S deep-sequencing analyses of the intestinal microbiome in each genotype at days five and twenty-nine. Of the 24 samples, 22 had sufficient read depth to allow us determine the overall composition of the gut bacterial microbiome. Principle component analysis (Fig. 1B), phylogenetic diversity metrics (Fig. 1C), and operational taxonomic unit (OTU) analysis (Fig. 1D) all suggest that inactivation of IMD in enterocytes had minimal impact on the composition or diversity of the intestinal microbiome at both time points. In contrast, inactivation of IMD in progenitors appears to affect the diversity (Fig. 1C) and relative OTU composition of the intestinal microbiome (Figure 1D), particularly at early stages. Here, we noted an increase in the representation of *Lactobacillus* OTUs in five day-old *esg^{ts}/D30A* intestines compared to age-matched *esg^{ts}/+* controls. In older intestines, we observed a reverse effect (Fig. 1D). In this case, the relative abundance of *Lactobacillus* OTUs was lower in *esg^{ts}>D30A* populations (mean abundance: 8.1%), than in all other genotypes (mean abundance: 15.2%). We then generated balance trees (39) to determine if cell-restricted inactivation of IMD affects the abundance of bacterial subcommunities within the microbiome. These studies identified a dominant balance, enriched with *Lactobacillales* and *Psudomonadales*, that distinguished five day-old *esg^{ts}/D30A* intestines from all other genotypes (Fig. 1E and F). Combined, these data suggest cell-dependent contributions of IMD to host associations with *Lactobacillus* species: inhibition of IMD in progenitor cells specifically affects the abundace of *Lactobacillus* OTUs, while inhibition of IMD in enterocytes appears to have negligible effects.

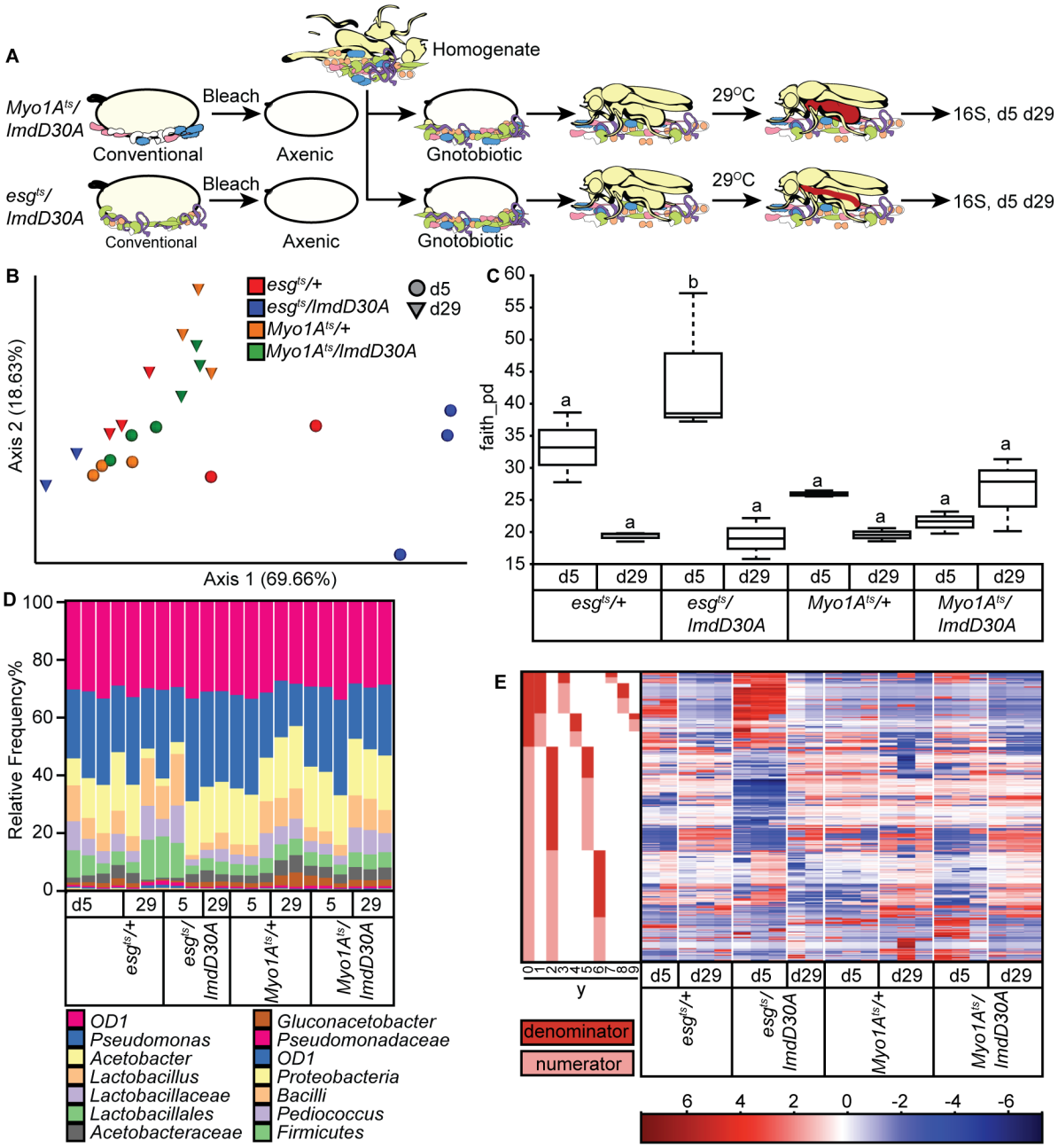

FIGURE 1. A: Generation of adult flies with similar populations of symbiotic bacteria. B: Principle component analysis of bacterial OTUs identified in flies of the indicated genotypes and ages. C: Faith phylogenetic diversity measurements of bacterial OTUs in flies of the indicated genotypes and ages. Letters above each genotype indicate groups that differ significantly from each other. D: Graphic illustration of replicate quantifications of OTUs in flies of the indicated ages and genotypes. E: Heatmap representation of relative bacterial OTU abundance in flies of the indicated ages and genotypes. F: Gneiss analysis was used to identify bacterial balances that differ between treatment groups. G: Bacterial genus abundance in the most significantly distinct bacterial balance.

Loss of IMD in progenitors affects association with symbiotic *Lactobacillus* species.

As IMD has cell specific effects on the representation of intestinal OTUs, we asked if progenitor or enterocyte-specific inactivation of IMD also affects total amounts of intestinal bacteria. For this experiment, we standardized the bacterial composition associated with each fly lines. Specifically, we generated axenic embryos of all genotypes to eliminate the endogenous microbiome, and poly-associated axenic adults with a 1:1:1 mix of three common fly symbionts – *Acetobacter pasteurianus* (*Ap*), *Lactobacillus brevis* (*Lb*), and *Lactobacillus plantarum* (*Lp*). To trace age-dependent changes in the microbiota of flies with compromised intestinal immune defenses, we measured bacterial loads in adult flies that we raised at 29°C for 1, 10, 20, or 30 days. Consistent with our deep-sequencing data, enterocyte-specific suppression of IMD did not affect the load of any tested bacterial species at any time points (Fig. S2A). Similarly, we did not observe measurable effects of IMD inhibition in progenitors on *Ap* loads at all times tested (Fig. S2B). In contrast, we detected age-dependent effects of IMD inhibition in progenitors on intestinal *Lactobacillus* numbers. Specifically, we detected significant decreases in the colony-forming units per fly of both *Lb* and *Lp* in esg^{ts}*/D30A* flies at 30 days compared to age-matched esg^{ts}*/+* controls (Fig. S3B). Combined with the data in Figure 1, our results suggest that IMD activity in progenitor cells contributes to host association with *Lactobacillus* symbionts as flies age.

Enterocyte IMD regulates metabolism and adult viability.

Given the cell-specific effects of IMD on pathogen virulence, microbiome diversity, and symbiont load, we hypothesized that the IMD pathway will also exert cell-specific controls on transcriptional events in the midgut. To test this hypothesis, we performed side by side RNA-sequencing analysis of midgut transcriptomes where we specifically inactivated IMD in enterocytes or in progenitors. We confirmed that expression of ImdD30A in enterocytes inhibits the expression of a *diptericin* reporter gene in the enterocytes, whereas expression of ImdD30A in progenitors does not impair *diptericin* expression in differentiated progeny, validating the utility of this approach to block IMD in targeted cells (Table S1). We then examined the transcriptomes of purified midguts from *Myo1A^{ts}/D30A* and control *Myo1A^{ts}/+* flies that we raised at 29°C for ten days (Fig. 2A). Inhibition of IMD in enterocytes had substantial effects on intestinal transcriptional activity (Fig. 2B, C), including on a cohort of immune effectors and modulators (Fig. S3A). We also found that inhibition of IMD in enterocytes had significant effects on processes as diverse as the control of cell shape, transport of metabolites, and metabolism of amino acids (Fig. 2D). The wide-ranging impacts on expression of metabolic regulators prompted us to ask if inhibition of IMD in enterocytes affects metabolism in the fly. To answer this question, we examined glucose, trehalose and lipid levels in the intestines and carcasses of *Myo1A^{ts}/D30A* and *Myo1A^{ts}/+* flies that we incubated at 29°C for ten days. Inhibition of enterocyte IMD did not affect glucose levels in the whole fly, or in the intestine (Fig. 2E and F). Likewise, inhibition of IMD in enterocytes did not affect trehalose, the main circulating disaccharide in the fly (Fig. 2G). In contrast, inhibition of IMD in enterocytes caused a significant increase of total (Figure 2H), and intestinal triglyceride levels (Fig. 2I), as well as an increase in adult weight (Fig. 2J). Interestingly, a loss of function mutation in *imd* decreased triglyceride levels (Fig. S3B), indicating enterocyte-specific roles for IMD in triglyceride storage. As enterocyte IMD modifies key processes such as metabolism in the intestine, we reasoned that inactivation of IMD will have consequences for intestinal physiology and animal viability. Consistent with this prediction, we found that blocking IMD in enterocytes impaired intestinal stem cell proliferation (Fig. 2K), and shortened adult lifespan (Fig. 2L). Combined, these results show that enterocyte IMD activity contributes to the regulation of adult metabolism and viability.

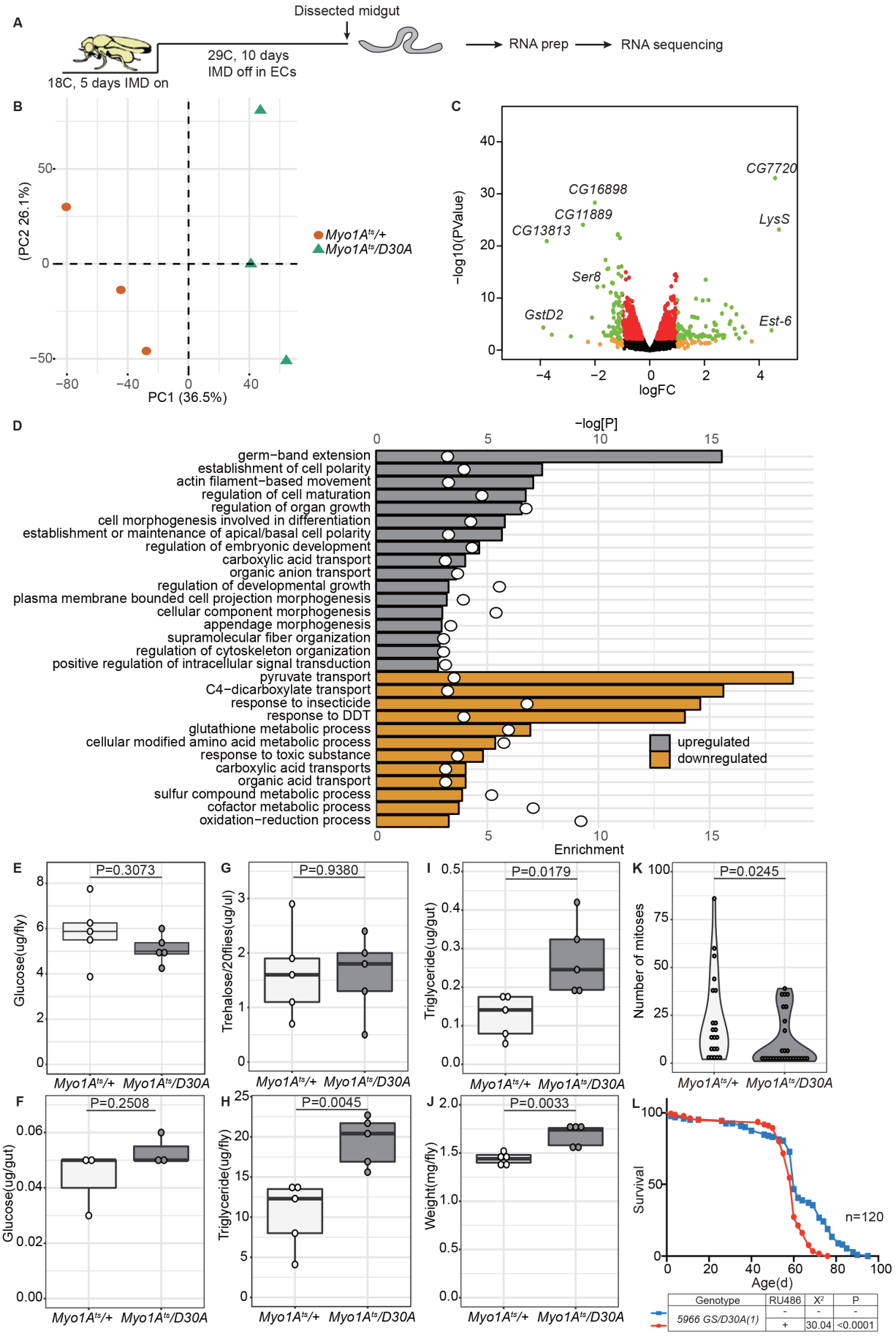

FIGURE 2. A: An experimental strategy for transcriptomic analysis of dissected midguts from flies with modified IMD activity. B: Principle component analysis of gene expression data for control flies (*Myo1A^{ts}/+*), and flies with IMD activity blocked in enterocytes (*Myo1A^{ts}/D30A*). C: Volcano plot of genes that are differentially expressed in *Myo1A^{ts}/D30A* midguts relative to *Myo1A^{ts}/+* midguts. Each point represents a single gene. Orange indicates genes with a greater than 2 fold-change in gene expression. Green indicates genes with a greater than 2 fold-change in gene expression, and an FDR below 0.01. D: Gene Ontology term analysis of pathways modified by inhibition of IMD in enterocytes. Column size indicates fold-enrichment, and circles show the significance of that enrichment on a negative log scale. E-J: Quantification of glucose (E-F), trehalose (G), triglyceride (H, I), and weight (J) of whole flies, or dissected midguts from flies of the indicated genotypes. P values are from significance tests performed with Student's t-tests for each measurement. K: Quantification of phospho-histone H3-positive mitotic cells in the posterior midguts of flies of the indicated genotypes raised at 29°C for 28 days. L: Survival curves of control flies (-), or flies with IMD activity blocked in enterocytes (+). N=number of flies for each genotype. Chi-squared and P values are from Log-rank tests.

Progenitor-specific roles for IMD.

In parallel to a transcriptional characterization of *Myo1A^{ts}/D30A* midguts, we determined the transcriptomes of purified midguts from *esg^{ts}/D30A* and *esg^{ts}/+* flies that we raised at 29°C for ten days. Again, we noticed significant impacts of IMD inhibition on transcriptional activity in the midgut (Fig. 3A and B). Examination of GO terms affected by inhibition of IMD in progenitors revealed a partial overlap with GO terms affected by inhibition of IMD in enterocytes, including genes linked to metabolism of amino acids or glutathione (Fig. 3C). However, IMD inhibition in progenitors had unique characteristics that were absent from the transcriptome of flies with inhibition of enterocyte IMD. For example inhibition of IMD in progenitors increased expression of genes involved in lipid catabolism and diminished expression of genes involved in RNA interference (Fig. 3C). In fact, greater than 30% of all genes impacted by IMD inhibition in progenitors were not affected by the inhibition of IMD in enterocytes (Fig. 3D and E), suggesting unique roles for progenitor cell IMD activity in the gut. A close examination

of genes differentially affected by inhibition of IMD in progenitors revealed substantial effects on immune response genes (Fig. 3F). We also noticed impacts on the expression of genes required for piRNA biogenesis; cholesterol absorption and signaling; the Notch, Wnt and JAK/STAT pathways; proteostasis; and regulation of adult lifespan (Fig. 3F). We consider these alterations to gene expression particularly interesting, as many of these pathways are involved in progenitor cell homeostasis and aging (40–42). In sum, our transcriptional studies reveal large differences between the contributions of enterocyte or progenitor cell IMD to intestinal homeostasis, and raise the possibility that progenitor cell IMD has unique roles in the regulation of intestinal stem cell function.

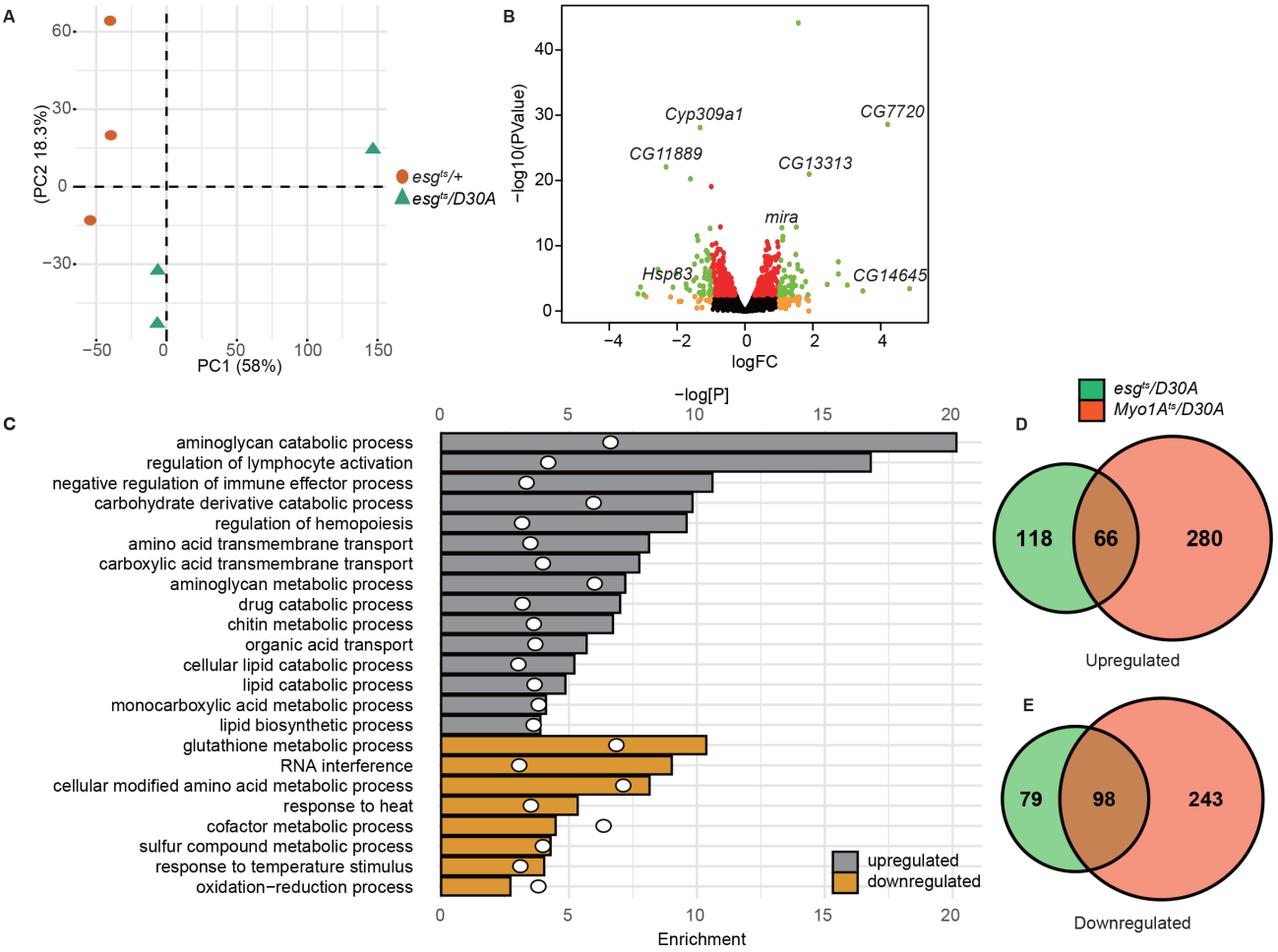

F

Gene	Function	logFC	P-value	Gene	Function	logFC	P-value	Gene	Function	logFC	P-value
IMMUNITY				**CHOLESTEROL**				**PROTEOSTASIS**			
imd	immunity	1.57	7.24E-45	*Hr96*	cholesterol signaling	0.48	8.72E-03	*Ero1L*	protein folding	-0.36	5.00E-03
LysS	immunity	1.18	2.07E-03	*Npc1b*	cholesterol absorption	0.86	4.20E-06	*Ugt*	protein folding	-0.37	1.69E-03
PGRP-SA	immunity	1.09	3.12E-05	*Npc2b*	cholesterol absorption	0.68	2.15E-05	*Der-1*	ERAD pathway	-0.67	1.95E-04
GILT2	immunity	1.03	4.64E-03	*Npc2e*	cholesterol absorption	0.68	2.03E-03	*meigo*	ER stress response	-0.42	2.83E-03
PGRP-SC1a	immunity	1.00	1.82E-07	*Npc1a*	cholesterol absorption	0.41	1.79E-03	*KdelR*	ER stress response	-0.29	6.53E-03
Tep3	immunity	0.88	8.41E-04	**SIGNALING**				*eca*	ER stress response	-0.31	3.27E-03
PGRP-SC1b	immunity	0.84	7.95E-07	*FoxK*	midgut development	-0.30	3.53E-03	*CCT1*	UPR	-0.34	2.28E-03
LysE	immunity	0.80	7.52E-03	*Gp93*	midgut development	-1.01	9.68E-04	*CCT8*	UPR	-0.35	4.77E-04
Rel	immunity	0.61	8.64E-03	*drl*	Wnt	0.41	9.55E-03	*nudC*	UPR	-0.36	5.19E-04
Tehao	immunity	0.57	2.70E-05	*sgg*	Wnt	0.31	2.76E-03	*Herp*	UPR	-0.58	2.63E-04
PGRP-LB	immunity	0.55	1.77E-04	*Cerk*	Wnt	-0.27	4.32E-03	*P58IPK*	UPR	-0.78	2.06E-03
Spn42Dd	immunity	0.55	1.37E-03	*Usp8*	Wnt	-0.32	2.21E-03	*Atg18b*	autophagy	0.75	4.77E-03
Pebp1	immunity	0.41	6.73E-03	*Cdc37*	Wnt	-0.36	5.96E-03	*Atg9*	autophagy	0.29	2.59E-03
Tep4	immunity	0.36	8.82E-04	*boca*	Wnt	-0.40	5.93E-03	*ced-6*	phagocytosis	0.55	8.73E-03
LRR	immunity	0.34	3.40E-03	*p24-1*	Wnt	-0.42	5.81E-03	*drpr*	phagocytosis	0.40	1.72E-03
cactin	immunity	-0.34	1.40E-03	*fz3*	Wnt	-0.46	5.06E-03	**LIFESPAN**			
Sherpa	immunity	-0.56	5.80E-05	*Sec22*	Wnt	-0.53	7.98E-04	*Indy*	metabolism	-0.35	2.44E-03
Vago	immunity	-1.48	6.12E-03	*ebd2*	Wnt	-0.62	2.94E-03	*Coq2*	metabolism	-0.37	5.26E-03
grass	immunity	-1.49	6.47E-08	*Su(var)2-10*	JAK/STAT	-0.32	2.08E-03	*alpha-Est7*	metabolism	-0.40	6.42E-03
Hayan	immunity	-1.63	6.66E-04	*et*	JAK/STAT	-0.72	5.19E-05	*tam*	DNA polymerase	-0.40	3.86E-03
IMPPP	immunity	-2.99	2.98E-03	*Hop*	JAK/STAT	-1.12	1.16E-08	*Cbs*	nitrite reducing	-0.41	4.11E-05
Mekk1	DUOX	0.46	1.54E-05	*kuz*	Notch	0.52	4.51E-03	*Tspo*	mitochondrial	-0.61	8.30E-05
p38c	DUOX	0.41	8.73E-03	*Nedd4*	Notch	0.42	1.59E-05	*Ccs*	SOD activity	-0.70	3.48E-07
PIRNA				*Fkbp14*	Notch	0.31	2.97E-03				
Ars2	piRNA biogenesis	-0.37	1.87E-03	*Nak*	Notch	0.28	6.35E-03				
pasha	piRNA biogenesis	-0.55	1.63E-03	*pzg*	Notch	-0.27	7.02E-03				
armi	piRNA biogenesis	-0.67	1.54E-04	*sno*	Notch	-0.28	6.18E-03				
vret	piRNA biogenesis	-0.79	9.57E-03	*pon*	Notch	-1.00	5.33E-03				

FIGURE 3. A: Principle component analysis of gene expression data for control flies (*esg^{ts}/+*), and flies with IMD activity blocked in progenitor cells (*esg^{ts}/D30A*). B: Volcano plot of genes that are differentially expressed in *esg^{ts}/D30A* midguts relative to *esg^{ts}/+* midguts. Each point represents a single gene. Orange indicates genes with a greater than 2 fold-change in gene expression. Green indicates genes with a greater than 2 fold-change in gene expression, and an FDR below 0.01. C: Gene Ontology term analysis of pathways modified by inhibition of IMD in progenitors. Column size indicates fold-enrichment, and circles show the significance of that enrichment on a negative log scale. D: Venn diagrams of overlap between genes that are upregulated, or downregulated, in *esg^{ts}/D30A* and *Myo1A^{ts}/D30A* as indicated. F: Table showing genes involved in immunity; piRNA biogenesis; cholesterol absorption and signaling; signal transduction; proteostasis; and longevity that are differentially regulated in *esg^{ts}/D30A* midguts relative to *esg^{ts}/+* midguts. Positive scores indicated genes that are upregulated in *esg^{ts}/D30A* midguts and negative scores indicate genes that are downregulated. All numerical values indicate fold-change on a $\log_2$ scale.

Inactivation of IMD in progenitors impairs intestinal homeostasis.

To determine how inhibition of IMD in progenitors affects the intestinal epithelium, we prepared a single-cell RNA sequencing profile of 1509 cells that we isolated from the intestines of *esg^{ts}/+* flies, and 1779 cells that we purified from *esg^{ts}/D30A* intestines (Fig. 4A). Looking at control, *esg^{ts}/+* flies we readily identified progenitor, endocrine, and enterocyte cell populations (Fig. 4B) that express markers of growth and differentiation (progenitors), gastrointestinal peptides (endocrine cells), and metabolic enzymes (enterocytes) (Fig. 4D). Examination of gene expression patterns in cells prepared from *esg^{ts}/D30A* intestines showed that expression of ImdD30A in progenitor cells had substantial impacts on epithelial homeostasis (Fig. 4C). For example, we detected a novel population of cells that expresses progenitor cell markers, such as Notch and headcase, but do not express *esg*. We have tentatively named these cells *hdc+, esg-* (Fig. 4C, E), and note that they also fail to express EGF and JAK/STAT pathway elements critical for progenitor growth, suggesting that this is an undifferentiated, non-proliferative cell type (Fig S4). Looking at differentiated cells, we observed the appearance of a fourth population

of posterior enterocytes, and a modest decline in endocrine numbers from 10% of all cells in *esg^{ts}/+* intestines to 7% of all cells in *esg^{ts}/D30A* intestines. Strikingly, changes to endocrine cells included a complete absence of the EE1 population (Fig. 4E), suggesting that IMD is required in progenitors for development of the secretory cell lineage.

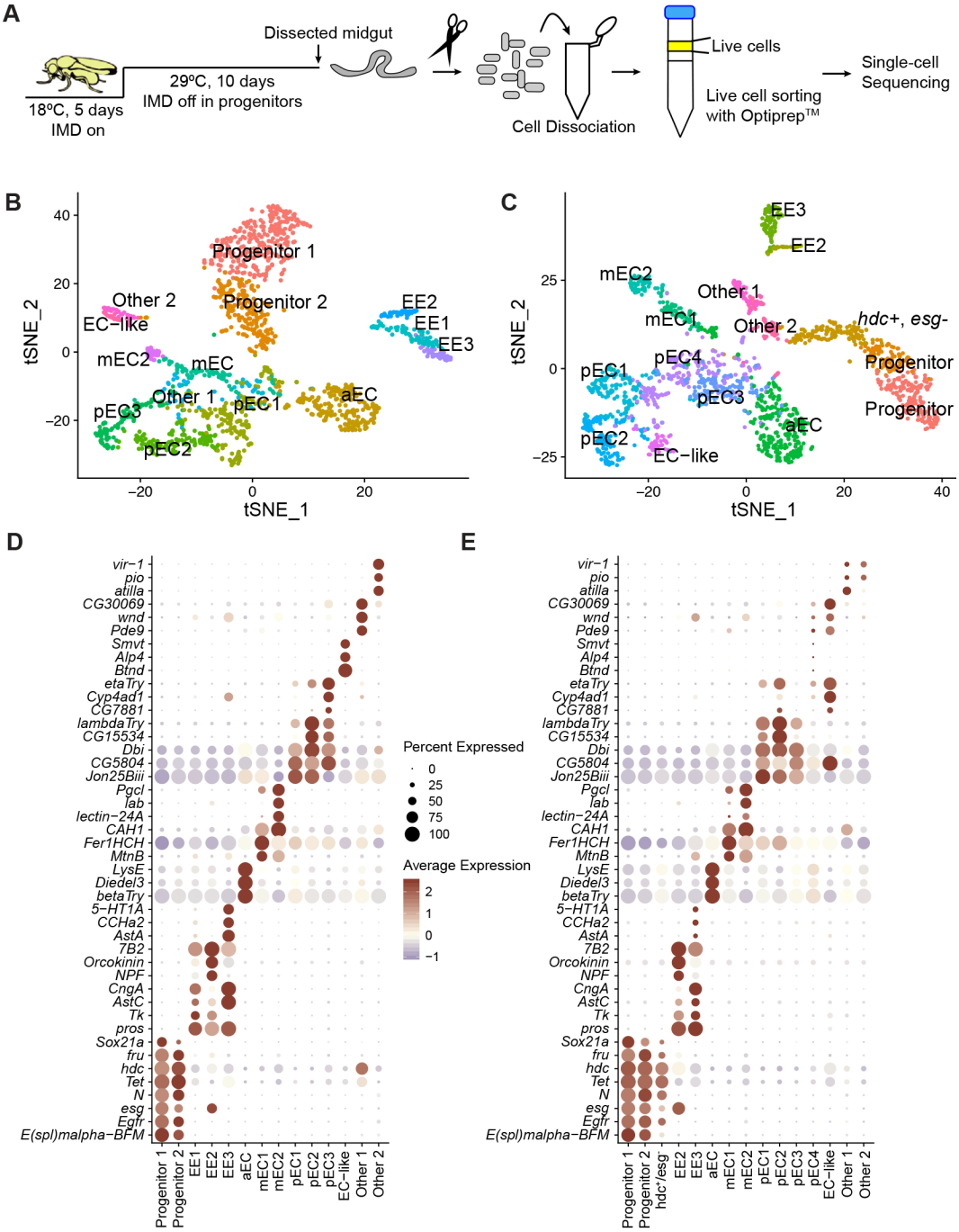

FIGURE 4. A: Strategy for the preparation of single-cell RNA expression atlases for an adult fly midgut. B-C: tSNE plots of cell-type clusters in the intestines of *esg^{ts}/+* (B), and *esg^{ts}/D30A* (C) flies. EC = enterocyte, EE =

enteroendocrine cell. D-E: Bubble plot of marker gene expression in indicated cells for *esg^{ts}/+* (D) and *esg^{ts}/D30A* (E) flies. Bubble size = percentage of cells that express the marker. Heatmap shows degree of expression.

When we examined gene ontology terms affected by IMD inhibition in progenitors, we noticed significant effects on the expression of genes required for growth and homeostasis in the progenitor compartment; for cell-cell contact and vesicle transport in endocrine cells; and for metabolic processes or transport in enterocytes (Figure 5A). Closer examination of differentially expressed genes confirmed that inhibition of IMD significantly impacted the expression of genes that contribute to progenitor cell adhesion and differentiation within the intestinal niche (Figure 5B). In endocrine cells, we observed a complete loss of expression of some peptide hormones, such as Allatostatin A (*AstA*), as well as ectopic expression of the Neuropeptide F (*NPF*) and Tachykinin (*Tk*) peptide genes in the EE3 population (Figure 5C), possibly as a compensation for the loss of EE1 cells. Finally, we found that inhibition of IMD in progenitor cells impacted the expression of prominent digestive, structural, and microbe-response genes in enterocyte populations (Figure 5D). Combined, the data presented in figures three to five implicate progenitor cell IMD in the maintenance of intestinal homeostasis.

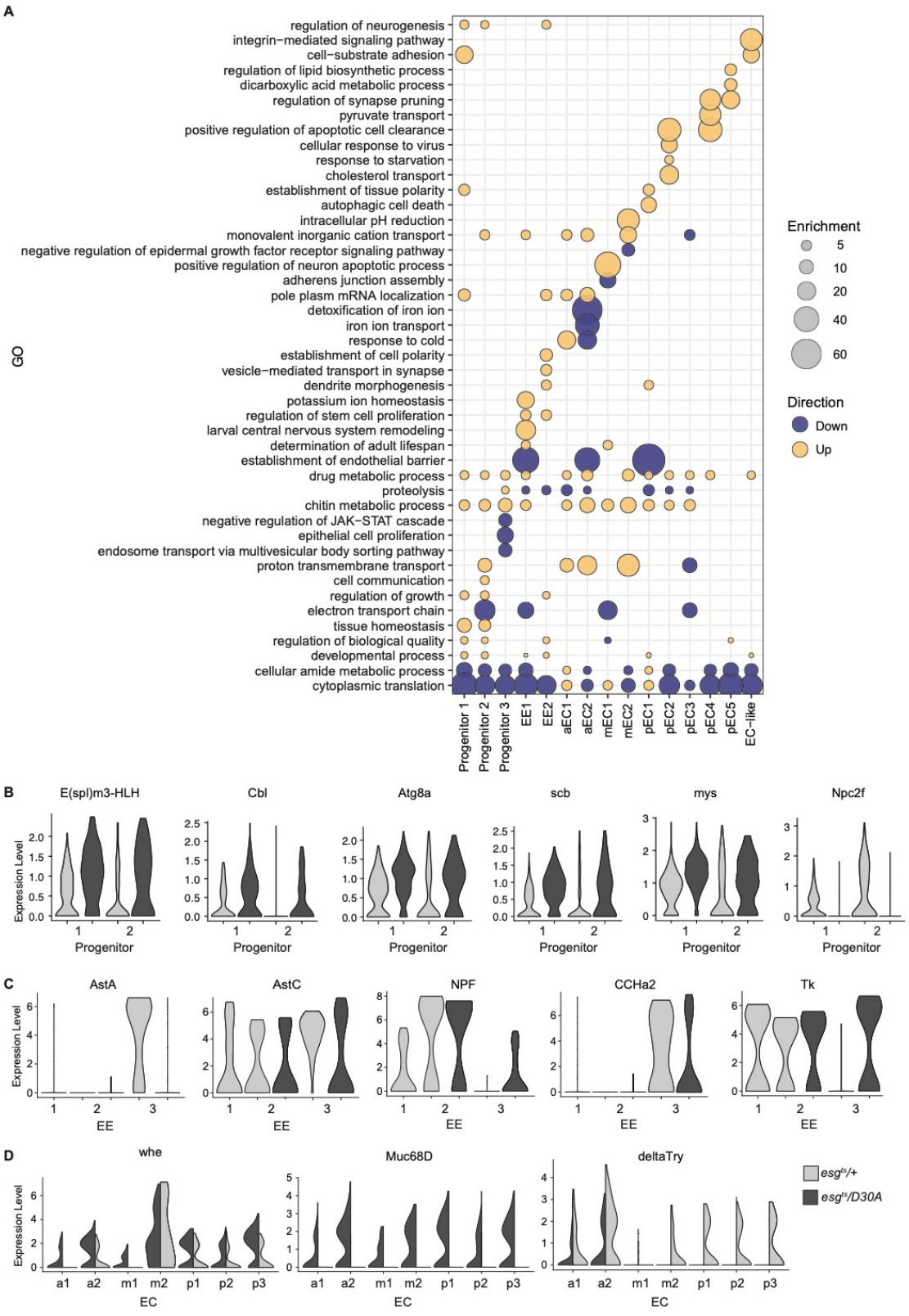

FIGURE 5. A: Bubble plot representation of GO terms differentially regulated in *esg*^{ts}*/D30A* cells relative to *esg*^{ts}*/+* cells. Bubble size indicate fold-enrichment of the respective terms. Color indicates upregulated or downregulated terms. B: Violin plots showing the expression of representative genes (Notch-response gene *E(spl)m3-HLH*; EGF

regulator *Cbl*; autophagy regulator *Atg8a*; integrins *scb* and *mys*, and cholesterol trafficker *Npc2f*) that were significantly differently expressed in *esg^{ts}/D30A* protenitor cells compared to *esg^{ts}/+* progenitors. C: Violin plots showing the relative expression of five endocrine peptides in *esg^{ts}/D30A* and *esg^{ts}/+* endocrine cell-types. D: Relative expression of the bacterial response gene *whe*, the mucin *Muc68D*, and the digestive enzyme *delta-Trypsin* in enterocytes of *esg^{ts}/D30A* and *esg^{ts}/+* intestines. All three are significantly differently expressed in *esg^{ts}/D30A* enterocytes compared to *esg^{ts}/+* enterocytes. For B-D. Gene expression values are normalized and log-transformed single cell expression values.

IMD activity in progenitors promotes stem cell proliferation and *Drosophila* viability.

To directly measure effects of IMD inhibition in progenitor cells on intestinal physiology, we quantified stem cell numbers in young and aged flies using Delta as a stem cell marker. We observed a significant decrease in the percent of Delta-positive cells in *esg^{ts}/D30A* flies compared to *esg^{ts}/+* control flies when flies were aged for 30 days (Fig. 6A). These results suggest that IMD activity is required for homeostatic ISC proliferation in adult flies. In agreement with this hypothesis, we detected a significant decrease in proliferating cells in *esg^{ts}/D30A* flies compared to *esg^{ts}/+* control flies (Fig. 6B).

Given the impacts of IMD inhibition on epithelial renewal and differentiation, we asked if progenitor-specific inhibition of IMD suppresses fly viability. For this experiment, we used the RU486-inducible GeneSwitch GAL4 system (37) to block IMD in progenitors. Using two independent *UASimdD30A* lines, we monitored the lifespans of control flies and flies with progenitor-specific suppression of IMD. In both cases, we found that flies died significantly faster when IMD was blocked in progenitors compared to their controls (Fig. 6 C and D). Taken together, our data indicate that IMD activity in the progenitor compartment protects the fly from pathogenic *Vibrio cholerae*, supports the growth of symbiotic *Lactobacillus* species, and contributes to epithelial growth and adult longevity.

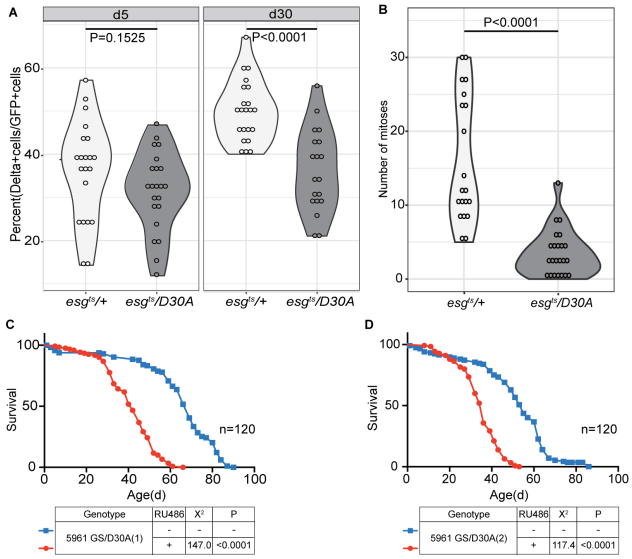

FIGURE 6. A: Percentage of cells positive for the stem cell marker, Delta in the posterior midgut of flies of the indicated genotypes and ages. P value are from a significance test performed with a Student's t-test. B: Quantification of phospho-histone H3-positive mitotic cells in the posterior midguts of 28d old flies of the indicated genotypes. P value are from a significance test performed with a Student's t-test. C-D: Survival curves of female control flies (-), or flies with IMD activity blocked in the progenitors (+). N=number of flies tested for each genotype. Chi-squared and P values are the results of Log-rank tests. Survival studies were performed with two distinct *imdD30A*-expressing flies (labeled 1 and 2, respectively).

DISCUSSION

To understand how intestinal defenses maintain animal health, it is important that we ask how immune activity in individual cell types contributes to gut homeostasis. We used *Drosophila melanogaster* to characterize the contributions of immune signaling in intestinal progenitors, or enterocytes, to intestinal homeostasis. Our study uncovered cell-specific contributions of IMD to host metabolism, intestinal growth, and survival of enteric infection. IMD has complex roles in the regulation of intestinal anti-bacterial responses (43). In the anterior, IMD activation in differentiated epithelial cells requires detection of cell-extrinsic, polymeric peptidoglycan by PGRP-LC (24). In the posterior midgut, IMD components are expressed and active in enterocytes and in progenitor cells (27–29), where IMD activation occurs upon detection of cytosolic, monomeric peptidoglycan by PGRP-LE (24, 25). Here, IMD contributes to the delamination of damaged epithelial cells (44), and the expression of immune-regulatory molecules (45). Alterations to IMD have been linked to effects on the size and composition of the gut microbiome (15, 17–20), and the lifespan of the fly (46–49). In the adult, IMD also has complex roles in responses to enteric infections. For example, IMD is necessary to survive infections with pathogenic *Serratia marcescens* (50), while IMD accelerates fly demise after infection with *Vibrio cholerae* (38).

At present, we know little about cell-specific aspects of IMD activity in the midgut. For example, several lines of evidence implicate IMD in metabolic homeostasis (17, 51–53). However, we don't know if these immune-metabolic links are cell-intrinsic, or if they are secondary to IMD-mediated changes to the gut microbiota, with attendant shifts in microbial control of metabolism in the host. Our results suggest that enterocyte IMD regulates host metabolism independent of the microbiome, as inhibition of enterocyte IMD does not influence bacterial numbers, or microbiome composition. Modification of enterocyte IMD also has effects on metabolism in distal sites, as inhibition of enterocyte IMD causes weight gain and hyperlipidemia in the adult. These observations align with a recent report that intestinal IMD influences fat body immune responses (54). We note that mutations in several IMD pathway genes are also linked to accelerated lipolysis in adult flies (55), further implicating the IMD pathway in the control and use of lipid stores.

The apparent absence of shifts in the microbiome after inhibition of enterocyte IMD was unexpected given the effects of IMD pathway mutations on the microbiota (15, 17–20). It is possible that IMD activity in intestinal regions not considered in this study such as the acidic copper cells may have more pronounced impacts on the microbiome. However, we note that a recent study reported similarities between the microbiome of conventionally reared flies, and immune-deficient *dif* ; *key* mutants (56). Furthermore, immune defects have minimal impacts on the gut microbiome of fish or mice (57, 58). In these models, familial transmission appear to be a major determinant of microbiome composition. As bacteria circulate from the food to the intestine in *Drosophila* (59), we consider it possible that mutations in IMD influence the recycling of symbiotic bacteria, possibly by altering feeding (55), with downstream consequences for the gut microbiome.

In contrast to enterocytes, inhibition of IMD in progenitors had detectable effects on symbiotic *Lactobacillus*. These observations match a recent characterization of flies with mutations in *PGRP-SD*, an IMD pathway modifier that is expressed in posterior midgut progenitor cells (27). Loss of PGRP-SD specifically affects intestinal levels of *Lactobacillus plantarum*, but does not affect *Acetobacter pomorum* levels. In the future, it will be interesting to see if the effects of IMD on intestinal *Lactobacillus* species are due to alterations in immune tolerance of *Lactobacillus* species, changes in the availability of metabolic intermediates required for bacterial growth, or a combination of those factors.

Mutational inactivation of IMD inhibitors, or chronic activation of IMD accelerates growth in the intestinal epithelium (46, 60, 61), although the mechanism remains unclear. Our work establishes IMD as an intrinsic regulator of progenitor growth; inhibition of IMD in the progenitor compartment results in a loss of intestinal progenitors, a decline in epithelial renewal, and mis-differentiation of the epithelium. We were particularly struck by the role of progenitor cell IMD in enteroendocrine cell development. We found that blocking IMD in progenitors led to a decline in total endocrine cell numbers, including loss of the *AstA*-positive EE1 population. These observations have parallels in zebrafish, mice, and rats, where removal of the gut microbiome results in a decline in endocrine numbers (34, 62, 63), suggesting an evolutionarily conserved requirement for bacterial response pathways in the development of secretory cell lineages. Recent studies implicate the vertebrate sensor of cytosolic

PGN, NOD2, in epithelial regeneration (31, 32), suggesting that immune-regulation of progenitor cell growth may be an evolutionarily conserved event. Our study does not determine if progenitor cell IMD regulates epithelial renewal by controlling progenitor viability, proliferation, or differentiation, and future experiments are required to address this question.

Finally, the cell-specific functions of IMD described in this study have consequences for the ability of adult flies to survive the enteric pathogen *Vibrio cholerae*. *imd* mutants survive *V. cholerae* infections longer than wild-type controls (38), indicating a role for IMD in host death. Inhibition of enterocyte IMD recapitulates this phenotype, while inhibition of IMD in progenitors has the opposite effect. These data suggest that enterocyte IMD contributes to *V. cholerae*-dependent killing of the fly, whereas progenitor cell IMD counters the effects of infection. Interestingly, neither phenotype results from changes in bacterial consumption, or the intestinal load of *V. cholerae*, suggesting that IMD directly affects the ability of flies to tolerate *V. cholerae*. As *V. cholerae* infections are sensitive to metabolite availability (64), and IMD has cell-specific effects on intestinal metabolism, we consider immune-mediated regulation of gut metabolism a candidate mechanism by which IMD influences survival after infection with *V. cholerae*.

In summary, our data suggest that enterocyte IMD influences intestinal, and systemic, metabolism in the fly. Loss of this activity impacts fly weight and lipid levels, and establishes an intestinal environment that favors *V. cholerae* pathogenesis. Progenitor cell IMD activity also affects the expression of metabolic pathway genes, albeit distinct to those controlled by IMD in enterocytes, and establishes an intestinal environment that extends host survival after infection with *V. cholerae*. In the absence of an infectious agent, inhibition of IMD in progenitor cells diminishes growth and renewal of intestinal progenitors, significantly shortening the lifespan of the fly. Given the evolutionary conservation of immune responses, we believe these data may be of relevance for understanding fundamental principles of immune-regulated intestinal homeostasis.

ACKNOWLEDGMENTS

Myo1A^{ts} flies and *esg*^{ts} were provided by Dr. Bruce Edgar, *dipt-cherry* flies were provided by Dr. Julien Royet, and Geneswitch lines were provided by Dr. Heinrich Jasper. The C6706 strain of *Vibrio cholerae* was provided by Dr. Stefan Pukatzki, and *Ecc15* was provided by Dr. Nicolas Buchon. This research was funded by a grant from the Canadian Institutes of Health Research to EF (MOP77746). AP was supported by an AIHS Summer Studentship. We acknowledge microscopy support from Dr. Stephen Ogg at the University of Alberta, and bioinformatics support from Meghan Ferguson and David Fast.

MATERIALS AND METHODS

Fly Husbandry

We used w^{1118} as a wildtype strain. We backcrossed *UAS-imdD30A* transgenic lines into the w^{1118} background for eight generations prior to use, and used standard fly husbandry methods to ensure that esg^{ts} (*esg-GAL4*, *tub-GAL80*^{ts}, *UAS-GFP*) flies had the same first and third chromosomes as our wild-type line. We maintained all fly stocks on standard corn meal medium (Nutri-Fly Bloomington formulation, https://bdsc.indiana.edu/information/recipes/bloomfood.html; Genesse Scientific). All experimental flies were adult virgin females kept under a 12h:12h light:dark cycle. The esg^{ts}*-GAL4, Myo1A*^{ts}*-GAL4* (*Myo1A-GAL4* ; *tub-GAL80*^{ts}, *UAS-GFP*)*, 5966 GS-GAL4* (RU-486-mediated expression of GAL4 in enterocytes)*,* and *5961 GS-GAL4* (RU-486-mediated expression of GAL4 in progenitor cells) flies were described previously (65–67). The pENTR/D-TOPO Imd construct used in this study was described elsewhere (68). We generated ImdD30A in a two-step site-directed mutagenesis PCR reaction using the following primers: imd-forward (CACCATGTCAAAGCTCAGGAACC), imdD30A-reverse (CCACGGGAGCTGCGGCCTTTTCCAGGCGTCCC), imdD30A-forward (GGGACGCCTGGAAAAGGCCGCAGCTCCCGTGG), imd-reverse (GGAGAAGCGCAAGACAAACAGCTAG). We sequenced the resultant clone to confirm the point mutation, and recombined it with pTW (LR recombination; Invitrogen) to generate a *UASImdD30A* plasmid. Transgenic lines were generated by Bestgene Inc. (CA, USA). To make axenic flies, we placed approximately 100 flies in a breeding cage with apple juice agar plates that contained yeast paste over night. The following morning, we collected eggs from the apple juice agar plates after visual inspection to confirm absence of larvae, and sterilized them by washing in a 10% solution of 7.4% sodium hypochlorite for 2.5min twice, followed by 1min wash with 70% EtOH, and three washes with autoclaved water. Working in a tissue-culture hood, we transferred axenic eggs to autoclaved standard fly food, and transferred vials to a decontaminated 21˚C incubator under a 12h:12h light:dark cycle. To confirm that flies were axenic, we regularly sampled the food, by resuspending in MRS (Difco *Lactobacilli* MRS Agar, DB, 288210) and plating onto MRS-agar plates that we checked for bacterial growth after 2-3 days at 29°C.

Adult infections with *V. cholerae*.

Thirty virgin female flies for each genotype were raised on standard food for 7d at 29°C, then infected with *V. cholerae* C6706 as described previously (31). Briefly, *V. cholerae* were spread on lysogeny broth (LB) agar plates and grown overnight at 37°C. The following morning, 30 flies of each genotype were distributed equally among three empty vials and starved for 2h prior to infection. We then suspended the overnight culture of *V. cholerae* in 10ml fresh LB, and diluted to an OD600 of 0.125. We transferred flies into vials that contained a third of a cotton plug soaked with 3ml of the overnight *V. cholerae* culture. Dead flies were counted every 8h without flipping onto fresh food.

Lifespan assay

For all longevity studies, we used the GeneSwitch (GS) gene expression system to inhibit IMD activity. This system has the advantage that control and experimental populations have identical genotypes. To activate the GS system, we added 100µl of RU486 (Mifepristone, M8046, Sigma) dissolved in 80% EtOH (4mg/ml) to the surface of standard food and dried overnight prior to addition of flies. For control flies, we added 100µl of 80% EtOH to the surface of standard food and dried overnight prior to addition of flies. For each treatment group, we placed thirty flies into four vials. All flies were maintained at 25˚C under a 12h:12h light:dark cycle throughout the experiment. We transferred flies to fresh food that contained either RU486, or vehicle, every Monday, Wednesday, and Friday, and counted dead flies at those times.

Establishment of poly-associated gnotobiotic adult *Drosophila*

We generated axenic flies as described above and starved flies for 2h prior to bacterial poly-association. To generate poly-associated gnotobiotic adults, we fed axenic flies a mix of three *Drosophila* symbiotic bacteria strains (*Lactobacillus plantarum*^{KP}, *Lactobacillus brevis*^{EF}, and *Acetobacter pasteurianus*^{AD}) that were isolated from our wild-type laboratory flies (31). Liquid cultures of each bacterial strain were prepared to an OD600 of 50 in 5% sucrose in PBS, then mixed at a 1:1:1 ratio. We placed 25 axenic flies per vial, into 5 vials that contained a quarter

of an autoclaved cotton plug soaked with 1ml of bacterial mixture, and fed flies the bacterial mix for 16h at 29°C. We then raised flies at 29°C on autoclaved standard fly food throughout the remainder of the experiment, transferring to fresh, autoclaved food every Monday, Wednesday, and Friday. To determine CFU, 25 flies were collected from each group and surface sterilized by successive washes in a 10% solution of 7.4% sodium hypochlorite, distilled water, 70% ethanol, and distilled water. Flies were randomly divided into groups of 5 and mechanically homogenized in 500µl MRS broth. We serially diluted homogenates in a 96-well plate, and plated 10µl spots on MRS agar to select for *Lactobacillus* species, or GYC agar to select for *Acetobacter pasteurianus*. Colonies were counted after 2 days growth at 29°C. We distinguished *L. plantarum* and *L. brevis* based on colony morphology: *L. plantarum* forms solid white, opaque colonies, while *L. brevis* colonies were large, round, irregular-edged, with an off-white center and translucent edges. To enumerate *V. cholerae* CFU, we used the procedure described above, working with 7d old virgin female adult flies that we infected with *V. cholerae* at 29°C for 24 hours prior to homogenization in LB buffer.

16S deep-sequencing library preparation.

For 16S deep-sequencing, we raised axenic fly embryos on autoclaved standard corn meal medium at 21°C. Axenic virgin females were selected, and fed a wild-type fly homogenate. To prepare the homogenate, we homogenized approximately 300 adult flies in 50ml 5% sucrose in PBS. We added 3ml of the homogenate to a third of a cotton plug (Fisher Scientific Canada 14127106) at the base of a clean vial. We transferred axenic flies to each vial (25 flies/vial) and fed flies the homogenate for 16h at 29°C. Flies were transferred to fresh, autoclaved food, and kept on autoclaved food for 5 days or 29 days at 29°C, flipping to fresh food weekly. Flies were surface sterilized, then bacterial DNA was extracted using the UltraClean Microbial DNA Isolation Kit (MO BIO Laboratories, Inc. Catalog #: 12224-250). Bacterial 16S DNA was amplified with PFX Taq (Invitrogen) using 16S pan-bacterial DNA primers (Forward: AGAGTTTGATCCTGGCTCAG, Reverse: GGCTACCTTGTTACGACTT), confirmed by electrophoresis, then purified with the QIAquick PCR Purification Kit (QIAGEN). We measured DNA concentration on Qubit 2.0 then used 1ng of DNA to generate a library with the Nextera PCR Master Mix (Illumina). Libraries were cleaned with

AMPure™ beads (QIAGEN), then pooled libraries were processed on the Illumina MiSeq platform with the MiSeq Reagent Kit v3 (600-cycle).

Feeding assay

We performed the Capillary Feeder (CAFE) assays as previously described (69). Briefly, we raised virgin females of the appropriate genotypes at 29˚C for 7d. We placed ten flies per vial into vials with three capillaries (calibrated Pipets (5ul, VWR, Cat No. 53432-706)) that contained liquid food with 8.1% sucrose (D-sucrose, Fisher BioReagents, BP220-212) and 1.9% yeast extract (BD, 212750). We measured consumption for ten vials for each genotype. At the same time, we maintained a control vial that contained three food-bearing capillaries, but no flies. To quantify food consumption per fly, we calculated (food consumed in vials that contained flies – food consumed in control vial that lacked flies)/number of flies per fly. For the FlyPad, virgin female adults were aged for 23-24 days at 29˚C (25 flies per vial) with weekly renewal of food. Prior to the assay, flies were starved on 1% (w/v) agar for 4h at 29˚C. Flies were placed into arenas (one fly per arena) with 3µl of food containing 8.1% sucrose, 1.9% yeast extract, and 1% agar. Feeding behavior was monitored for 1 hour as described previously (70).

Metabolic assay

For metabolic measurements, adult virgin females were raised on standard medium for 10d at 29˚C. We measured the combined weight of five adult flies then mechanically homogenized in TE buffer (10mM Tris, pH 7.4, 1mM EDTA pH 8.0, 0.1% Triton X-100). Homogenates were used for measuring total triglyceride using the Serum TG Determination Kit (TR0100; Sigma) and total glucose by the GAGO Glucose Assay Kit (GAGO20; Sigma) following the manufacturer's instructions. We performed the same assays with 9-10 dissected intestines from adult virgin females. To measure circulating trehalose, 20 adult flies per sample were punctured on the thorax and spun at 9000 rcf for 5min at 4˚C through a filter tube (Zymo Research, C1006-50-F). Hemolymph was mixed in the trehalase buffer (5 mM Tris pH 6.6, 137 mM NaCl, 2.7 mM KCl) at a 1:100 dilution and heated at 70˚C for 5 min. We divided mixtures into two groups, and one was treated with Porcine Kidney Trehalase (T8778-1UN; Sigma), and another

group was not. Both groups were incubated at 37˚C for 22h and treated with glucose assay reagent (GAGO20; Sigma) for 30min at 37˚C. To stop the reaction, we added 12N sulfuric acid and measured absorbance at 540nm.

Immunofluorescence

We used previously described immunofluorescence protocols to visualize posterior midguts (56). In brief, we used anti-phospho-histone H3 (PH3, 1:1000, Millipore (Upstate), 06-570) immunofluorescence to quantify mitoses in the midguts, and anti-Delta (1:100; Developmental Studies Hybridoma Bank C594.9B) immunofluorescence to quantify stem cells in the R4/R5 region of the posterior midguts of virgin female flies that we raised at 29˚C for 5d or 30d. For DNA staining we used Hoechst 33258 (1:500; Molecular Probes) and the appropriate secondary antibody are goat anti-mouse Alexa Fluor 647 (1:500,Invitrogen) and 568 (1:500, Invitrogen) and goat anti-rabbit Alexa Fluor 488 (1:1000, Invitrogen) and 546 (1:1300, Invitrogen). Guts were mounted on slides in Fluoromount (Sigma-Aldrich F4680), and the posterior midgut was visualized with a spinning disk confocal microscope (Quorum WaveFX; Quorum Technologies Inc.). Images were collected as z-slices and processed with Fiji software to generate a single z-stacked image.

Bioinformatics

Statistical analyses for metabolic assays, longevity studies, and survival analyses were performed with GraphPad Prism. Survival data and longevity data were analyzed with Log-rank (Mantal-Cox) tests. Feeding assays, CFU, quantification of PH-3 or Delta positive cells, and metabolic assays were analyzed with unpaired Student's t-tests. Survival, and longevity curves were generated by GraphPad Prism and the R programming language was used for remaining figures. All figures were assembled using Adobe Illustrator. We used QIIME2-2019.1 for all analysis of 16S data, filtering all sequences that were present below a minimum frequency of 200, and using the DADA2 package for sequence quality control. We binned sequences at 99% sequence identity, and used the greengenes database to identify operational taxonomic units. Differential abundance analysis was performed using the gneiss plugin for QIIME2. RNAseq was performed with RNA purified by TRIZOL (ambion, 15596-026) purification from

the midguts of adult flies that we raised at 29°C for 10d. Purified RNA was sent on dry ice to Novogene (CA, USA) for library construction and sequencing with Illumina Platform PE150. For RNAseq studies, we obtained approximately 40 million reads per biological replicate. We used FASTQC to evaluate the quality of raw, paired-end reads, and trimmed adaptors and reads of less than 36 base pairs in length from the raw reads using Trimmomatic version 0.36. We used HISAT2 version 2.1.0 to align reads to the *Drosophila* transcriptome- bdgp6, and converted the resulting BAM files to SAM flies using Samtools version 1.8. We counted converted files using Rsubread version 1.24.2 and loaded them into EdgeR. In EdgeR, we filtered genes with counts less than 1 count per million and normalized libraries for size. Normalized libraries were used to call genes that were differentially expressed among treatments. Genes with P-value < 0.01 and FDR < 0.01 were defined as differentially expressed. Principle component analysis was performed on normalized libraries using Factoextra version 1.0.5, and Gene Ontology enRIchment anaLysis and visuaLizAtion tool (GORILLA) was used to determine Gene Ontology (GO) term enrichment. Specifically, differentially expressed genes were compared in a two-list unraked comparison to all genes output from edgeR as a background set, and redundant GO terms were removed. For single cell analysis, Cell Ranger v3.0 was used to align sequencing reads to the *Drosophila* reference transcriptome (FlyBase, r6.30) and generate feature-barcode matrices. These matrices were analyzed using the Seurat R package (version 3.1.1). Cells possessing <500 UMIs or >2500 UMIs were removed to reduce the number of low-quality cells and doublets. Seurat was then used to normalize expression values and perform cell clustering at a resolution of 0.8 with 7 principal components. Clusters were identified based on known markers and previous single-cell analysis of the *Drosophila* intestine (https://www.flyrnai.org/scRNA/). For GO term analysis of single cell data, Seurat was used to integrate *esg/+* and *esg/D30A* datasets and generate lists of differentially expressed genes for each cluster. Both up- and down-regulated gene lists (p-value cut-off <0.05) were analyzed in GOrilla to determine GO term enrichment. Differentially expressed genes were compared in a two-list unranked comparison to all genes identified in the single-cell dataset. GO terms were then analyzed in REVIGO (REduce and VIsualize Gene Ontology) to remove

redundant GO terms. Top enriched GO terms are shown for each cluster, as well as those same GO terms found in other clusters.

Data availability

Gene expression data have been submitted to the NCBI GEO database (GEO: GSE135154).

CITATIONS

1. Hooper L V. (2015) Epithelial Cell Contributions to Intestinal Immunity. *Advances in Immunology* doi:10.1016/bs.ai.2014.11.003.

2. Allaire JM, et al. (2018) The Intestinal Epithelium: Central Coordinator of Mucosal Immunity. *Trends Immunol*. doi:10.1016/j.it.2018.04.002.

3. Miguel-Aliaga I, Jasper H, Lemaitre B (2018) Anatomy and physiology of the digestive tract of drosophila melanogaster. *Genetics*. doi:10.1534/genetics.118.300224.

4. Ohlstein B, Spradling A (2006) The adult Drosophila posterior midgut is maintained by pluripotent stem cells. *Nature* 439(7075):470–474.

5. Micchelli CA, Perrimon N (2006) Evidence that stem cells reside in the adult Drosophila midgut epithelium. *Nature*. doi:10.1038/nature04371.

6. Perdigoto CN, Schweisguth F, Bardin AJ (2011) Distinct levels of Notch activity for commitment and terminal differentiation of stem cells in the adult fly intestine. *Development*. doi:10.1242/dev.065292.

7. Ohlstein B, Spradling A (2007) Multipotent Drosophila intestinal stem cells specify daughter cell fates by differential notch signaling. *Science (80-)*. doi:10.1126/science.1136606.

8. Biteau B, Jasper H (2014) Slit/Robo Signaling Regulates Cell Fate Decisions in the Intestinal Stem Cell Lineage of Drosophila. *Cell Rep*. doi:10.1016/j.celrep.2014.05.024.

9. Zeng X, Hou SX (2015) Enteroendocrine cells are generated from stem cells through a distinct progenitor in the adult Drosophila posterior midgut. *Development*. doi:10.1242/dev.113357.

10. Guo Z, Ohlstein B (2015) Bidirectional Notch signaling regulates Drosophila intestinal stem cell multipotency. *Science (80-)*. doi:10.1126/science.aab0988.

11. Liu X, Hodgson JJ, Buchon N (2017) Drosophila as a model for homeostatic, antibacterial, and antiviral mechanisms in the gut. *PLoS Pathog*. doi:10.1371/journal.ppat.1006277.

12. Jiang H, Edgar BA (2012) Intestinal stem cell function in Drosophila and mice. *Curr Opin Genet Dev*. doi:10.1016/j.gde.2012.04.002.

13. Jiang H, et al. (2009) Cytokine/Jak/Stat Signaling Mediates Regeneration and Homeostasis in the Drosophila Midgut. *Cell*. doi:10.1016/j.cell.2009.05.014.

14. N. L, et al. (2008) PIMS Modulates Immune Tolerance by Negatively Regulating Drosophila Innate Immune Signaling. *Cell Host Microbe*. doi:10.1016/j.chom.2008.07.004.

15. Buchon N, Broderick NA, Chakrabarti S, Lemaitre B (2009) Invasive and indigenous microbiota impact intestinal stem cell activity through multiple pathways in Drosophila. *Genes Dev*. doi:10.1101/gad.1827009.

16. Myllymäki H, Valanne S, Rämet M (2014) The Drosophila Imd Signaling Pathway . *J Immunol*. doi:10.4049/jimmunol.1303309.

17. Broderick NA, Buchon N, Lemaitre B (2014) Microbiota-induced changes in Drosophila melanogaster host gene expression and gut morphology. *MBio*. doi:10.1128/mBio.01117-14.

18. Broderick NA, Lemaitre B (2012) Gut-associated microbes of Drosophila melanogaster. *Gut Microbes*. doi:10.4161/gmic.19896.

19. Ryu JH, et al. (2008) Innate immune homeostasis by the homeobox gene Caudal and commensal-gut mutualism in Drosophila. *Science (80-)*. doi:10.1126/science.1149357.

20. Clark RI, et al. (2015) Distinct Shifts in Microbiota Composition during Drosophila Aging Impair Intestinal Function and Drive Mortality. *Cell Rep*. doi:10.1016/j.celrep.2015.08.004.

21. Buchon N, Broderick NA, Poidevin M, Pradervand S, Lemaitre B (2009) Drosophila Intestinal Response to Bacterial Infection: Activation of Host Defense and Stem Cell Proliferation. *Cell Host Microbe*. doi:10.1016/j.chom.2009.01.003.

22. Ryu J-H, et al. (2004) The Homeobox Gene Caudal Regulates Constitutive Local Expression of Antimicrobial Peptide Genes in Drosophila Epithelia. *Mol Cell Biol*. doi:10.1128/mcb.24.1.172-185.2004.

23. Capo F, Charroux B, Royet J (2016) Bacteria sensing mechanisms in Drosophila gut: Local and systemic consequences. *Dev Comp Immunol*. doi:10.1016/j.dci.2016.01.001.

24. Bosco-Drayon V, et al. (2012) Peptidoglycan sensing by the receptor PGRP-LE in the Drosophila gut

induces immune responses to infectious bacteria and tolerance to microbiota. *Cell Host Microbe*. doi:10.1016/j.chom.2012.06.002.

25. Neyen C, Poidevin M, Roussel A, Lemaitre B (2012) Tissue- and Ligand-Specific Sensing of Gram-Negative Infection in Drosophila by PGRP-LC Isoforms and PGRP-LE . *J Immunol*. doi:10.4049/jimmunol.1201022.

26. Kaneko T, et al. (2006) PGRP-LC and PGRP-LE have essential yet distinct functions in the drosophila immune response to monomeric DAP-type peptidoglycan. *Nat Immunol*. doi:10.1038/ni1356.

27. Iatsenko I, Boquete JP, Lemaitre B (2018) Microbiota-Derived Lactate Activates Production of Reactive Oxygen Species by the Intestinal NADPH Oxidase Nox and Shortens Drosophila Lifespan. *Immunity*. doi:10.1016/j.immuni.2018.09.017.

28. Fink C, et al. (2016) Intestinal FoxO signaling is required to survive oral infection in Drosophila. *Mucosal Immunol*. doi:10.1038/mi.2015.112.

29. Dutta D, et al. (2015) Regional Cell-Specific Transcriptome Mapping Reveals Regulatory Complexity in the Adult Drosophila Midgut. *Cell Rep*. doi:10.1016/j.celrep.2015.06.009.

30. Li Y, et al. (2014) Constitutive TLR4 signalling in intestinal epithelium reduces tumor load by increasing apoptosis in APC Min/+ mice. *Oncogene*. doi:10.1038/onc.2012.581.

31. Nigro G, Rossi R, Commere PH, Jay P, Sansonetti PJ (2014) The cytosolic bacterial peptidoglycan sensor Nod2 affords stem cell protection and links microbes to gut epithelial regeneration. *Cell Host Microbe*. doi:10.1016/j.chom.2014.05.003.

32. Zanello G, et al. (2016) The Cytosolic Microbial Receptor Nod2 Regulates Small Intestinal Crypt Damage and Epithelial Regeneration following T Cell–Induced Enteropathy. *J Immunol*. doi:10.4049/jimmunol.1600185.

33. Neal MD, et al. (2012) Toll-like receptor 4 is expressed on intestinal stem cells and regulates their proliferation and apoptosis via the p53 up-regulated modulator of apoptosis. *J Biol Chem*. doi:10.1074/jbc.M112.375881.

34. Troll J V., et al. (2018) Microbiota promote secretory cell determination in the intestinal epithelium by

modulating host Notch signaling. *Development*. doi:10.1242/dev.155317.

35. Cheesman SE, Neal JT, Mittge E, Seredick BM, Guillemin K (2011) Epithelial cell proliferation in the developing zebrafish intestine is regulated by the Wnt pathway and microbial signaling via Myd88. *Proc Natl Acad Sci U S A*. doi:10.1073/pnas.1000072107.

36. Paquette N, et al. (2010) Caspase-Mediated Cleavage, IAP Binding, and Ubiquitination: Linking Three Mechanisms Crucial for Drosophila NF-κB Signaling. *Mol Cell*. doi:10.1016/j.molcel.2009.12.036.

37. McGuire SE, Mao Z, Davis RL (2004) Spatiotemporal Gene Expression Targeting with the TARGET and Gene-Switch Systems in Drosophila. *Sci Signal*. doi:10.1126/stke.2202004pl6.

38. Berkey CD, Blow N, Watnick PI (2009) Genetic analysis of Drosophila melanogaster susceptibility to intestinal Vibrio cholerae infection. *Cell Microbiol*. doi:10.1111/j.1462-5822.2008.01267.x.

39. Morton JT, et al. (2017) Balance Trees Reveal Microbial Niche Differentiation. *mSystems*. doi:10.1128/msystems.00162-16.

40. Rodriguez-Fernandez IA, Qi Y, Jasper H (2019) Loss of a proteostatic checkpoint in intestinal stem cells contributes to age-related epithelial dysfunction. *Nat Commun*. doi:10.1038/s41467-019-08982-9.

41. Obniski R, Sieber M, Spradling AC (2018) Dietary Lipids Modulate Notch Signaling and Influence Adult Intestinal Development and Metabolism in Drosophila. *Dev Cell*. doi:10.1016/j.devcel.2018.08.013.

42. Sousa-Victor P, et al. (2017) Piwi Is Required to Limit Exhaustion of Aging Somatic Stem Cells. *Cell Rep*. doi:10.1016/j.celrep.2017.08.059.

43. Zhai Z, Huang X, Yin Y (2018) Beyond immunity: The Imd pathway as a coordinator of host defense, organismal physiology and behavior. *Dev Comp Immunol*. doi:10.1016/j.dci.2017.11.008.

44. Zhai Z, Boquete JP, Lemaitre B (2018) Cell-Specific Imd-NF-κB Responses Enable Simultaneous Antibacterial Immunity and Intestinal Epithelial Cell Shedding upon Bacterial Infection. *Immunity*. doi:10.1016/j.immuni.2018.04.010.

45. Zaidman-Rémy A, et al. (2006) The Drosophila Amidase PGRP-LB Modulates the Immune Response to Bacterial Infection. *Immunity*. doi:10.1016/j.immuni.2006.02.012.

46. Paredes JC, Welchman DP, Poidevin M, Lemaitre B (2011) Negative regulation by Amidase PGRPs shapes the drosophila antibacterial response and protects the Fly from innocuous infection. *Immunity*. doi:10.1016/j.immuni.2011.09.018.

47. Fernando MDA, Kounatidis I, Ligoxygakis P (2014) Loss of Trabid, a New Negative Regulator of the Drosophila Immune-Deficiency Pathway at the Level of TAK1, Reduces Life Span. *PLoS Genet*. doi:10.1371/journal.pgen.1004117.

48. Libert S, Chao Y, Chu X, Pletcher SD (2006) Trade-offs between longevity and pathogen resistance in Drosophila melanogaster are mediated by NFκB signaling. *Aging Cell*. doi:10.1111/j.1474-9726.2006.00251.x.

49. Morris O, et al. (2016) Signal Integration by the IκB Protein Pickle Shapes Drosophila Innate Host Defense. *Cell Host Microbe*. doi:10.1016/j.chom.2016.08.003.

50. Nehme NT, et al. (2007) A model of bacterial intestinal infections in Drosophila melanogaster. *PLoS Pathog*. doi:10.1371/journal.ppat.0030173.

51. Davoodi S, et al. (2019) The Immune Deficiency Pathway Regulates Metabolic Homeostasis in Drosophila . *J Immunol*. doi:10.4049/jimmunol.1801632.

52. Combe BE, et al. (2014) Drosophila microbiota modulates host metabolic gene expression via IMD/NF-κB signaling. *PLoS One*. doi:10.1371/journal.pone.0094729.

53. Musselman LP, et al. (2017) A Complex Relationship between Immunity and Metabolism in Drosophila Diet-Induced Insulin Resistance . *Mol Cell Biol*. doi:10.1128/mcb.00259-17.

54. Yang S, et al. (2019) Sugar Alcohols of Polyol Pathway Serve as Alarmins to Mediate Local-Systemic Innate Immune Communication in Drosophila. *Cell Host Microbe*. doi:10.1016/j.chom.2019.07.001.

55. Molaei M, Vandehoef C, Karpac J (2019) NF-κB Shapes Metabolic Adaptation by Attenuating Foxo-Mediated Lipolysis in Drosophila. *Dev Cell*. doi:10.1016/j.devcel.2019.04.009.

56. Mistry R, Kounatidis I, Ligoxygakis P (2017) Interaction between familial transmission and a constitutively active immune system shapes gut microbiota in Drosophila melanogaster. *Genetics*.

doi:10.1534/genetics.116.190215.

57. Ubeda C, et al. (2012) Familial transmission rather than defective innate immunity shapes the distinct intestinal microbiota of TLR-deficient mice. *J Exp Med*. doi:10.1084/jem.20120504.

58. Stagaman K, Burns AR, Guillemin K, Bohannan BJM (2017) The role of adaptive immunity as an ecological filter on the gut microbiota in zebrafish. *ISME J*. doi:10.1038/ismej.2017.28.

59. Blum JE, Fischer CN, Miles J, Handelsman J (2013) Frequent replenishment sustains the beneficial microbiome of Drosophila melanogaster. *MBio*. doi:10.1128/mBio.00860-13.

60. Petkau K, Ferguson M, Guntermann S, Foley E (2017) Constitutive Immune Activity Promotes Tumorigenesis in Drosophila Intestinal Progenitor Cells. *Cell Rep*. doi:10.1016/j.celrep.2017.07.078.

61. Guo L, Karpac J, Tran SL, Jasper H (2014) PGRP-SC2 promotes gut immune homeostasis to limit commensal dysbiosis and extend lifespan. *Cell*. doi:10.1016/j.cell.2013.12.018.

62. Kandori H, Hirayama K, Takeda M, Doi K (1996) Histochemical, Lectin-Histochemical and Morphometrical Characteristics of Intestinal Goblet Cells of Germfree and Conventional Mice. *Exp Anim*. doi:10.1538/expanim.45.155.

63. Uribe A, Alam M, Johansson O, Midtvedt T, Theodorsson E (1994) Microflora modulates endocrine cells in the gastrointestinal mucosa of the rat. *Gastroenterology*. doi:10.1016/0016-5085(94)90526-6.

64. Hang S, et al. (2014) The acetate switch of an intestinal pathogen disrupts host insulin signaling and lipid metabolism. *Cell Host Microbe*. doi:10.1016/j.chom.2014.10.006.

65. Nicholson L, et al. (2008) Spatial and temporal control of gene expression in drosophila using the inducible geneSwitch GAL4 system. I. Screen for larval nervous system drivers. *Genetics*. doi:10.1534/genetics.107.081968.

66. Buchon N, Broderick NA, Kuraishi T, Lemaitre B (2010) Drosophila EGFR pathway coordinates stem cell proliferation and gut remodeling following infection. *BMC Biol*. doi:10.1186/1741-7007-8-152.

67. Ren F, et al. (2010) Hippo signaling regulates Drosophila intestine stem cell proliferation through multiple pathways. *Proc Natl Acad Sci*. doi:10.1073/pnas.1012759107.

68. Guntermann S, Foley E (2011) The protein Dredd is an essential component of the c-Jun N-terminal kinase pathway in the Drosophila immune response. *J Biol Chem*. doi:10.1074/jbc.M111.220285.

69. Diegelmann S, et al. (2017) The CApillary FEeder Assay Measures Food Intake in Drosophila melanogaster. *J Vis Exp*. doi:10.3791/55024.

70. Itskov PM, et al. (2014) Automated monitoring and quantitative analysis of feeding behaviour in Drosophila. *Nat Commun*. doi:10.1038/ncomms5560.

SUPPLEMENTARY MATERIAL

Adult infections with *Ecc15*.

For septic infection experiments, we grew an overnight culture of *Ecc15* in LB, at 29°C, shaking. We pelleted the overnight culture in 1.5ml microfuge tubes and maintained it on ice. Anesthetized female flies were stabbed under the wing with a needle dipped into the bacterial pellet, control flies were stabbed with a needle dipped into LB. Infected flies were transferred to vials containing regular food overnight. Quantitative PCR (qPCR) measurements were performed with TRIZOL-purified RNA from whole flies (10 per replicate), and we used the $\Delta\Delta$ cycle threshold method to calculate relative expression values. Gene expressions were normalized to actin. The following primers were used in this study: diptericin (F: ACCGCAGTACCCACTCAATC, R: ACTTTCCAGCTCGGTTCTGA), and actin (F: TGCCTCATCGCCGACATAA, R: 59-CACGTCACCAGGGCGTAAT).

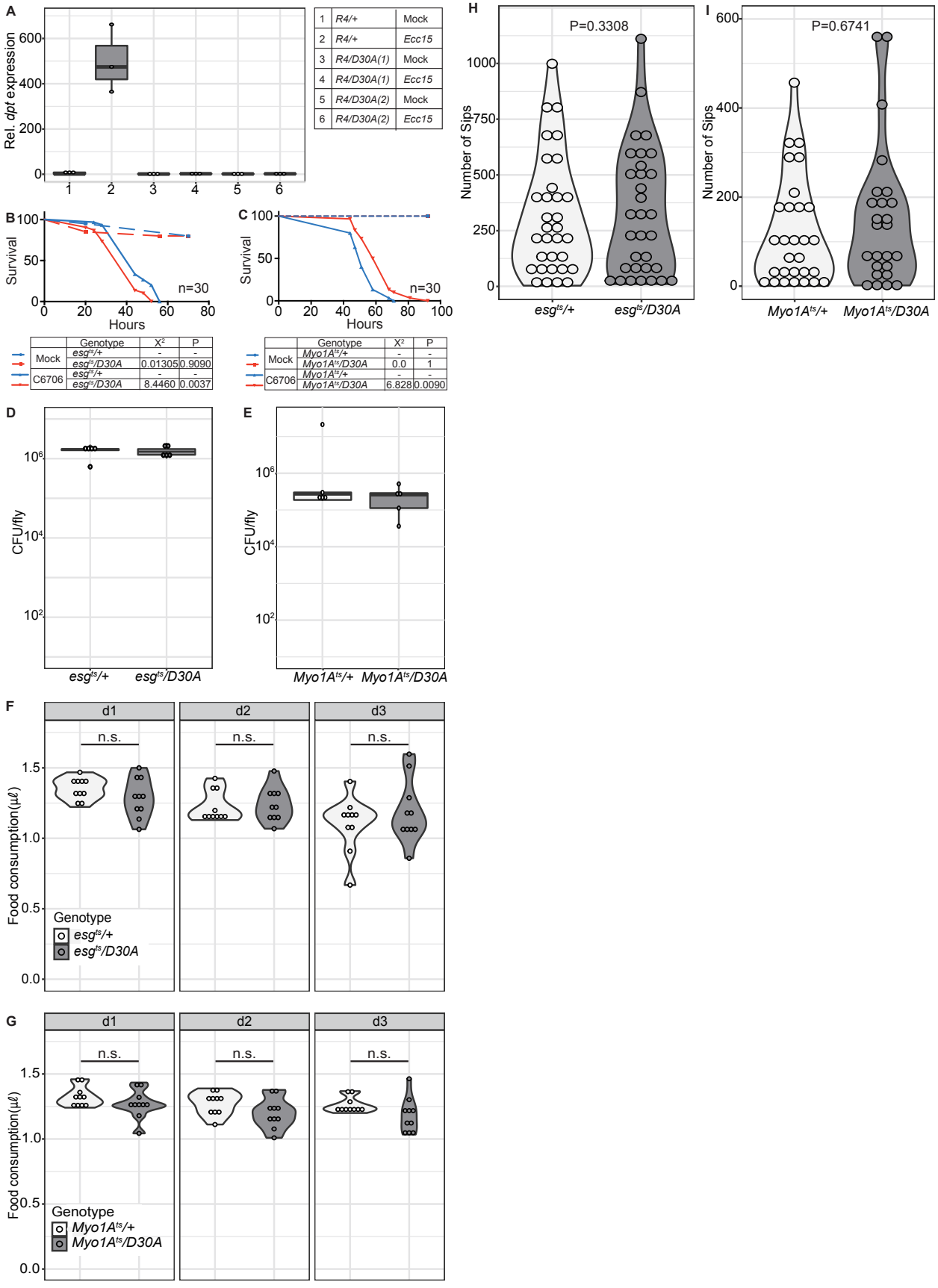

FIGURE S1. A: qPCR measurement of *dpt* expression in uninfected (mock), or *Ecc15*-infected (*Ecc15*) adult control flies (*R4/+*), or flies that express *imdD30A* in the fat body (*R4/D30A*). Infection experiments were performed with two distinct *imdD30A*-expressing transgenic flies (labeled 1 and 2, respectively). B-C: Survival curves of uninfected (mock), or *V. cholerae*-infected (C6706) adult flies of the indicated genotypes. N=number of flies in each treatment group. Chi-squared and P values are the results of Log-rank tests. D-E: CFU/fly of *V. cholerae* in adult flies of the indicated genotypes 24 h after infection with the C6706 strain of *V. cholerae*. F-G: Food consumption rates per adult flies of the indicated genotypes, measured in a CAFÉ assay for the indicated period of days. (H-I) Quantification of total feeding number of sips in adult flies of the indicated genotypes. All flies were raised at 29°C for 23 days prior to the assay, and each point represents the results for a single fly. P-values show the results of unpaired Student's t-tests.

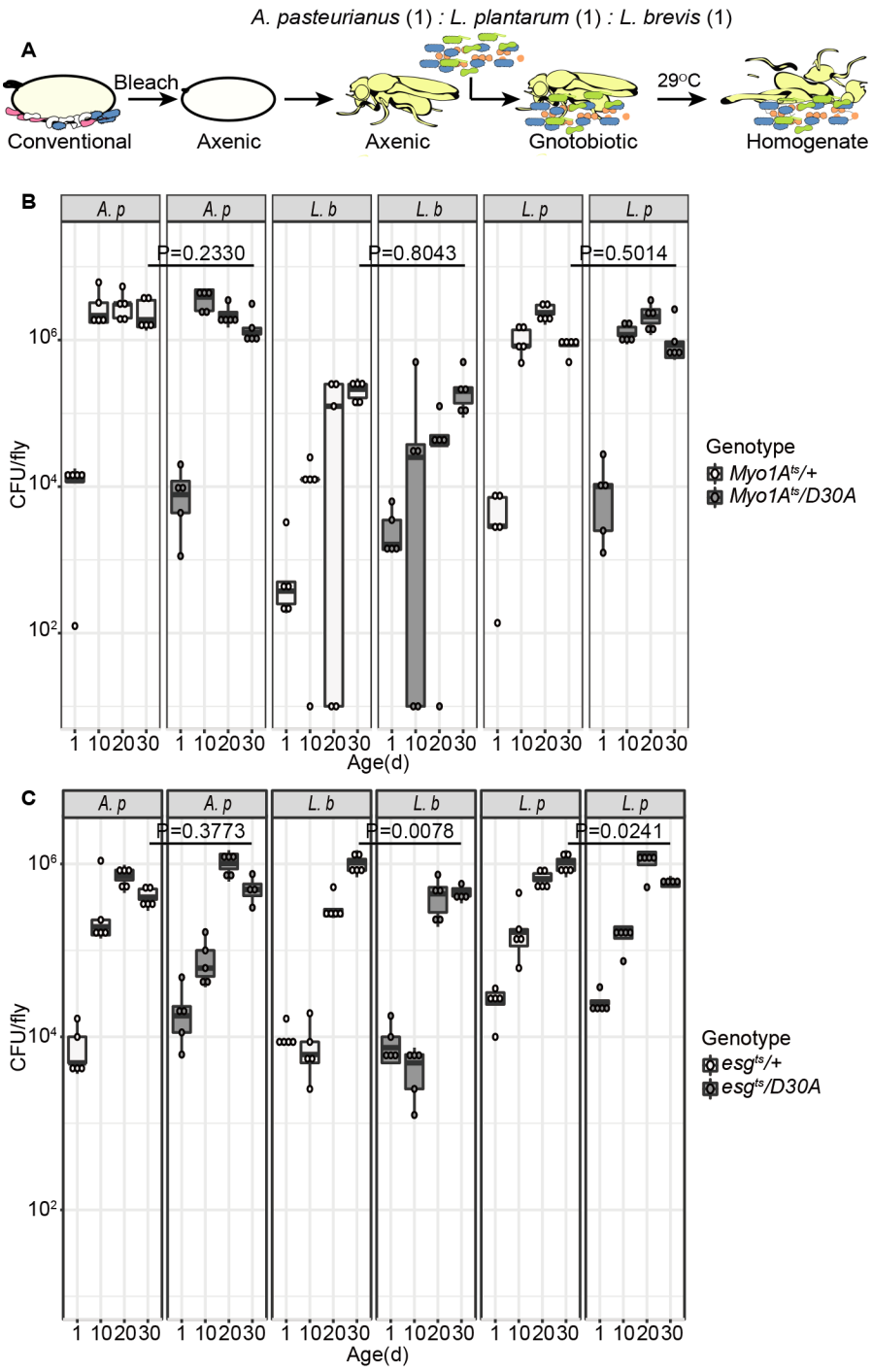

FIGURE S2. A: Schematic representation of an experimental strategy for generation of gnotobiotic flies. B-C: Quantification of *Acetobacter pateurianus* (*A.p.*), *Lactobacillus brevis* (*L.b.*), and *Lactobacillus plantarum* (*L.p.*) levels in the intestines of flies of the indicated genotypes raised at 29°C for the indicated duration.

A

IMMUNITY			
Gene	logFC	PValue	FDR
AttD	-2.88	2.32E-03	2.32E-02
grass	-1.31	6.30E-07	4.10E-05
Sherpa	-0.51	2.95E-04	5.14E-03
PGRP-LC	-0.36	2.71E-03	2.57E-02
cactin	-0.28	8.87E-03	6.06E-02
GILT1	0.15	3.33E-01	5.81E-01
LRR	0.46	5.49E-05	1.44E-03
PGRP-LB	0.48	1.14E-03	1.39E-02
Tep4	0.52	1.05E-06	6.30E-05
Mekk1	0.55	1.56E-07	1.26E-05
IMPPP	0.61	5.18E-01	7.35E-01
p38c	0.64	4.82E-05	1.30E-03
PGRP-SC1b	0.67	8.00E-05	1.95E-03
Tehao	0.73	5.50E-08	5.08E-06
Rel	0.73	1.66E-03	1.82E-02
LysE	0.81	6.80E-03	4.96E-02
PGRP-SA	0.82	8.94E-04	1.16E-02
Vago	0.83	8.74E-02	2.67E-01
PGRP-SC1a	0.84	1.13E-05	4.36E-04
GILT2	0.94	7.09E-03	5.12E-02
LysS	4.72	6.98E-24	9.48E-21

B

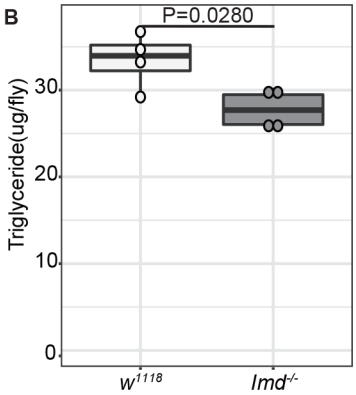

FIGURE S3: Quantification of relative changes in immune gene expression for *Myo1A^{ts}/D30A* flies relative to *Myo1A^{ts}/+* flies. All measurements were taken from RNAseq data shown in Figure 2, and show the average change on a $\log_2$-fold scale for three biological replicates, as well as P-values and FDR for each gene. Quantification of total triglyceride levels in flies of the indicated genotype raised on a holidic diet for 20 days.

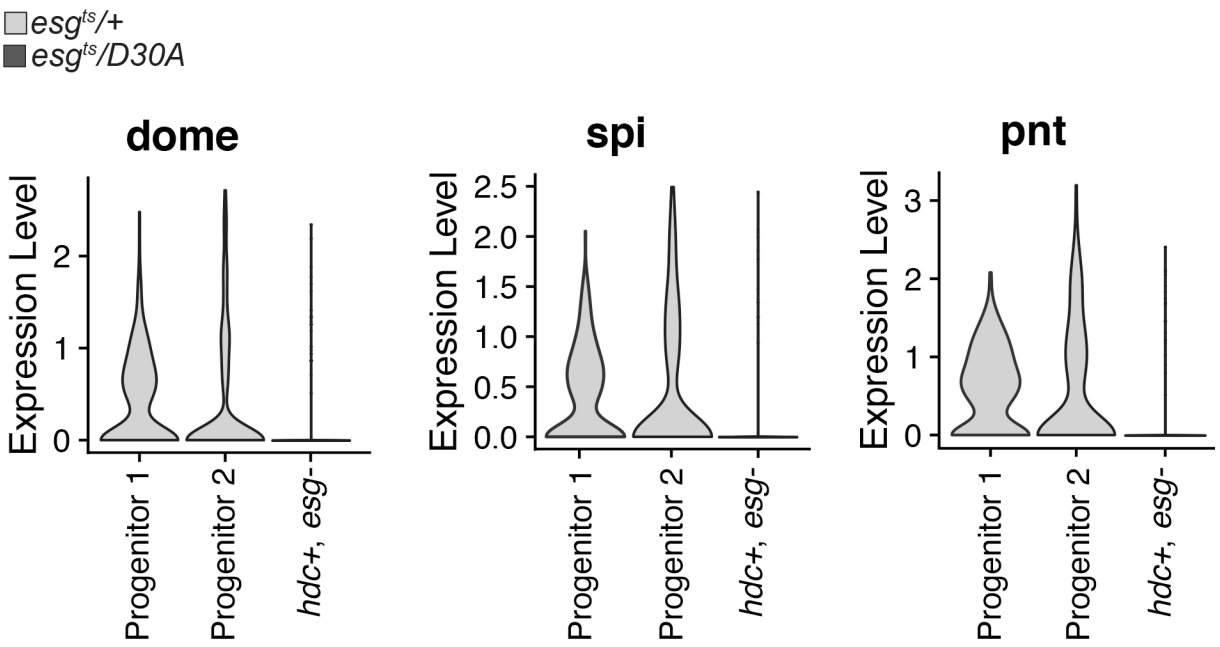

FIGURE S4. Violin plots showing the expression of the JAK/STAT activating receptor *dome*, the *Drosophila* EGF homolog, *spi*, and the *Drosophila* EGF pathway transcription factor *pnt*. Data are drawn from the single-cell sequencing profiles presented in Figures 4 and 5. For all three genes, expression is evident in progenitor populations 1 and 2 in *esg^{ts}/+* flies, but not detected in *hdc+*, *esg-* cells from *esg^{ts}/D30A* flies.

Genotype	Total number of guts	Number of dipt expressed guts	Percent (%)
esg^{ts}-GAL4/+; dipt-Cherry/+	12	12	100
esg^{ts}-GAL4/+; dipt-Cherry/ImdD30A	12	12	100
Myo1A^{ts}-GAL4/+; dipt-Cherry/+	10	10	100
Myo1A^{ts}-GAL4/+; dipt-Cherry/ImdD30A	15	4	26.67

TABLE S1. Quantification of expression of a *diptericin*-RFP reporter gene in the enterocytes of flies of the indicated genotypes that we infected with *Ecc15.* Expression of ImdD30A in enterocytes (*Myo1A^{ts}/+* ; *diptCherry/ImdD30A*) inhibits immune reporter expression in the enterocyte, whereas expression of ImdD30A in progenitors (*esg^{ts}/+* ; *diptCherry/ImdD30A*) does not.